Supporting Information for:

RAFT Aqueous Dispersion Polymerization yields Poly(ethylene glycol)-Based Diblock Copolymer Nano-objects with Predictable Single Phase Morphologies

Nicholas J. Warren, Oleksandr O. Mykhaylyk, Daniel Mahmood, Anthony J. Ryan and Steven P. Armes*

Department of Chemistry, University of Sheffield, Brook Hill, Sheffield, S3 7HF, UK

Experimental

Materials

4,4'-Azobis(4-cyanovaleric acid) (ACVA, V-501; 99%), *N*-hydroxysuccinimide (NHS; 98%), dicyclohexylcarbodiimide (DCC; 99%), 2,2'-azobis(2-methylpropionamide) dihydrochloride (AIBA; 97%), 4-cyano-4-(phenylcarbonothioylthio)pentanoic acid (CPADB; 97%), monomethoxy-capped poly(ethylene glycol) (average M_n = 5000 g mol^{-1}) and methanesulfonyl chloride (≥ 99.7%) were purchased from Sigma Aldrich (UK). 2,2'-Azobis[2-(2-imidazolin-2-yl)propane]dihydrochloride (AIPD, VA-044) was purchased from Wako Pure Chemical Industries, Ltd (Osaka, Japan). Deuterated methanol (CD_3OD, 99.96 atom %) was purchased from Goss Scientific (Nantwich, UK). Solvents were obtained from Fisher Scientific (Loughborough, UK) and were used as received.

Methods

Synthesis of 4-cyano-4-((thiobenzoyl)sulfanyl)pentanoic succinimide ester (SCPDB)

4-Cyano-4-(phenylcarbonothioylthio)pentanoic acid (CPADB, 2.04 g, 7.3 mmol) and *N*-hydroxysuccinimide (0.84 g, 7.3 mmol) were co-dissolved in anhydrous dichloromethane (15 mL). Dicyclohexylcarbodiimide (DCC) (1.51 g, 7.3 mmol) was added to this solution and the reaction mixture was stirred at 20°C in the dark for 18 h. An insoluble white by-product was removed by filtration. The remaining solution was concentrated using a rotary evaporator, and the resulting liquid was purified by silica column chromatography using a mixed eluent comprising 4:1 v/v *n*-hexane/ethyl acetate. A red solid was isolated after evaporation of the solvent (yield = 2.50 g, 91%).

Synthesis of mono-aminated poly(ethylene glycol)$_{113}$ (PEG-NH_2)

This precursor was prepared by adapting a literature protocol.[47] PEG_{113}-OH (average M_n= 5000 g mol^{-1}, 50.0 g, 10.0 mmol) was dissolved in 500 mL anhydrous toluene and azeotropically distilled under a nitrogen atmosphere to remove approximately 300 mL of this solvent. After cooling to 20°C, the flask was placed in an ice bath and anhydrous

dichloromethane (approximately 200 mL) was gradually added until the solution became clear. Triethylamine (2.13 mL, 1.52 g 15.0 mmol) was added dropwise with stirring, followed by the dropwise addition of mesyl chloride (1.71 g, 1.18 mL, 15.0 mmol). After 18 h, the reaction solution was filtered to remove the insoluble white triethylamine hydrochloride salt, followed by precipitation into excess diethyl ether. The off-white PEG_{113}-OMs product (47 g) was isolated by filtration and dried under vacuum.

The PEG_{113}-Ms intermediate (45.0 g) was added to a 25% aqueous ammonia solution (300 mL) in a 1 L duran bottle. The lid was tightly sealed with the aid of Parafilm^R and the reaction solution was stirred for four days at 20^{o}C. The lid was subsequently removed and the ammonia was allowed to evaporate slowly over three days at the back of a fumehood. NaOH (5 M) was added dropwise to the solution until the pH reached 13 and the polymer was extracted into dichloromethane (3 x 100 mL). The combined organics were washed with brine and subsequently dried over anhydrous magnesium sulfate. After concentrating under vacuum, the crude PEG_{113}-NH_2 product was precipitated into excess diethyl ether and dried under vacuum to produce PEG_{113}-NH_2 (43.0 g). The presence of the primary amine end-group was indicated by a triplet at δ 2.9 ppm by ^{1}H NMR spectroscopy, which corresponds to the two methylene protons adjacent to the amine. Comparison of this integrated triplet with that of the peaks corresponding to the protons on the PEG backbone indicated more than 98% amine end-group functionality.

Synthesis of poly(ethylene glycol) dithiobenzoate (PEG_{113}-DB) macro-CTA

Before carrying out the reaction, all glassware was rigorously dried at 120°C overnight to remove all traces of water. SCPDB (3.50 g, 9.3 mmol) was dissolved in anhydrous dichloromethane (20 mL) in a 100 mL two-neck round-bottomed flask fitted with a dropping funnel. A solution of dried PEG_{113}-NH_2 (39.5 g, 7.9 mmol) in dichloromethane (100 mL) was added dropwise to the SCPDB solution over a period of approximately 1 h. This reaction solution was stirred overnight, precipitated into excess diethyl ether and the resulting pink polymer (PEG_{113}-DB) was analyzed by ^{1}H NMR spectroscopy. The

presence of aromatic signals at δ 7.4 – 7.9 confirmed the presence of the desired terminal dithioester group and comparison of these integrated signals with that at δ 3.0 – 4.0 due to the ethylene glycol protons of the PEG chain suggested approximately 93 % functionalization. Visible spectroscopy was also used to determine the dithiobenzoate content of the PEG chains, using a calibration curve constructed from a series of methanolic solutions containing varying concentrations of CPADB. From this plot, a molar extinction coefficient of 104 800 ± 640 L mol^{-1} cm^{-1} was calculated for the absorption maximum observed at 516 nm in methanolic solution (see Figure S3). Using this information, a mean degree of dithiobenzoate functionalization of 97 ± 2 % was calculated for three separate PEG_{113}-DB batches.

RAFT dispersion polymerization of HPMA using the PEG_{113}-DB macro-CTA

The following representative protocol was used for the synthesis of PEG_{113}-$PHPMA_{300}$ at 10 % w/w solids using AIPD initiator at 50°C. AIPD initiator (0.0025 g, 0.0077 mmol), PEG_{113}-DB macro-CTA (0.1225 g, 0.0231 mmol; [CTA]/[AIPD] molar ratio = 3.0) and HPMA monomer (1.00 g, 6.94 mmol, target DP = 300) were weighed into a round-bottomed flask containing a magnetic stir bar. These reagents were dissolved in previously deoxygenated water (10.13 mL, 10% w/w) and purged with nitrogen for 30 minutes. The flask was sealed using a rubber septum under a positive nitrogen flow and immersed in an oil bath at 50°C. For the kinetic studies, aliquots were periodically removed for analysis by ^{1}H NMR spectroscopy and GPC. When the polymerization had proceeded for 2.5-3 h, the reaction was quenched by exposure to air and cooling to 20°C.

Dynamic light scattering (DLS)

DLS measurements were conducted at 25°C using a Malvern Instruments Zetasizer Nano series instrument equipped with a 4 mW He-Ne laser operating at 633 nm, an avalanche photodiode detector with high quantum efficiency, and an ALV/LSE-5003 multiple tau digital correlator electronics system. Light scattering was detected at 173°

and hydrodynamic diameters were determined using the Stokes-Einstein equation, which assumes spherical, non-interacting, perfectly monodisperse particles.

Nuclear magnetic resonance spectroscopy

^{1}H NMR spectra were acquired using either a Bruker 250 MHz or a 400 MHz spectrometer.

Samples were dissolved in $CDCl_3$, CD_2Cl_2 or CD_3OD at 10-20 mg mL^{-1}. All chemical shifts are reported in ppm (δ). The average number of scans accumulated per spectrum was typically 64.

Visible absorption spectroscopy

A PC-controlled Perkin-Elmer Lambda 25 spectrophotometer was used for recording spectra at 20°C from 400 nm to 700 nm at a scan rate of 240 nm min^{-1} and a slit width of 1 nm.

Gel permeation chromatography (GPC)

The GPC set-up comprised two 5 μm Mixed-C columns; a WellChrom K-2301 refractive index detector operating at 950 ± 30 nm and a Precision detector PD 2020 light scattering detector (with scattering angles of 90º and 15º). THF eluent contained 2.0% v/v triethylamine and 0.05% w/v butylhydroxytoluene (BHT) and a flow rate of 1.0 mL min^{-1} was employed. A series of ten near-monodisperse poly(methyl methacrylate) standards (M_p ranging from 1,280 to 330,000 g mol^{-1}) were employed as calibration standards in conjunction with the above refractive index detector.

Transmission electron microscopy (TEM)

Copper/palladium TEM grids (Agar Scientific) were surface-coated in-house to produce a thin film of amorphous carbon. The grids were then plasma glow-discharged for 30 seconds to create a hydrophilic surface. After glow discharge, the grids were immersed in 0.10% w/v aqueous dispersions containing the diblock copolymer nano-objects for 40

seconds. After blotting to remove excess sample dispersion, the grids were negatively stained by immersion in uranyl formate solution (0.75% w/v) for 30 seconds. The grid was blotted again to remove excess stain and dried using a vacuum hose. This heavy metal salt acts as a negative stain to improve electron contrast. Imaging was performed using a FEI Tecnai Spirit TEM instrument equipped with a Gatan 1kMS600CW CCD camera operating at 120 kV.

Rheology measurements

An AR-G2 rheometer equipped with a variable temperature Peltier plate, a 40 ml 2° aluminium cone and a solvent trap was used for all experiments. Loss modulus (G") and storage modulus (G') were measured as a function of percentage strain and temperature to map the linear viscoelastic region and also to determine the critical gelation temperature (CGT). Percentage strain sweeps were conducted at constant temperature (5°C) using an angular frequency of 1.0 rad s^{-1}. Angular frequency sweeps were carried out at a constant strain of 1.0 %. Temperature sweeps were conducted at a constant angular frequency of 1.0 rad s^{-1} and a constant strain of 1.0 %. In this latter experiment, the temperature was increased by 1.0 °C between each measurement, allowing an equilibration time of 10 minutes in each case. The solvent trap was required to prevent evaporation of water over the timescale of the experiment.

Small angle X-ray scattering (SAXS).

SAXS patterns have been recorded at a synchrotron source (ESRF, station ID02, Grenoble, France) at room temperature (21 °C) using monochromatic X-ray radiation (wavelength λ = 0.0995 nm) and a 2D FReLoN Kodak CCD detector (frame exposure time 0.1 s). Depending on requirements either two camera length setups (9.1 m and 3 m covering q range from 0.01 nm^{-1} to 2.0 nm^{-1}, where $q = \frac{4\pi \sin\theta}{\lambda}$ is the length of the scattering vector and θ is a half of the scattering angle) or one camera length setup (3 m, q range 0.03 - 0.2 nm^{-1}) was used for the data collection. A solution cell with

removable mica windows was used as a sample holder. The sample was poured into the solution cell and a mica window was placed on top. This loading protocol avoided shear effects, which could otherwise occur if the sample was injected into the cell. A multi-frame approach with a frame rate of 10 Hz was used for SAXS data collection. This acquisition method enables stability of samples exposed to X-ray beam to be monitored. It has been noticed that in some cases a long exposure time (for more than 100 ms) to the X-ray beam, heating the sample locally, couses changes in the SAXS pattern. Scattering data reduced by SAXS utilities software package (integration, normalization, background subtraction and patterns merging) were further analyzed using either Irena SAS macros for Igor Pro[1] or SASfit program[2].

Simple structural models based mainly on shape form factors of scattering objects are applied for SAXS analysis. For example, given that the X-ray scattering length densities of the blocks comprising the copolymer are similar, the SAXS patterns of the PEG_{113}-$PHPMA_{100}$ spherical micelles can be fitted reasonably well by a relatively simple model based on a spherical form factor (see Figure 7f and the main text associated with this figure). This can be demonstrated by comparing results obtained from this model to results obtained from a more sophisticated micelle model.[3, 4] Assuming that there is no penetration of the PEG coronal blocks in the PHPMA micelle core, the following expression for the spherical micelle form factor can be used[3, 4]:

$$F_{mic}(q) = N_{agg}^2 \beta_s^2 A_s^2(q, R_s) + N_{agg} \beta_c^2 F_c(q, R_g) + N_{agg}(N_{agg} - 1)\beta_c^2 A_c^2(q) + 2N_{agg}^2 \beta_s \beta_c A_s A_c(q) \quad \text{(S1)}$$

where R_s is the radius of the micelle core and R_g is the radius of gyration of the PEG corona block. The X-ray scattering length contrasts for the PHPMA core block and the PEG corona block are $\beta_s = V_s(\xi_s - \xi_{sol})$ and $\beta_c = V_c(\xi_c - \xi_{sol})$, respectively. ξ_s, ξ_c, and ξ_{sol} are X-ray scattering length densities for the core block (ξ_{PHPMA} = 11.11 × 10^{10} cm^{-2}), corona block (ξ_{PEG} = 11.37 × 10^{10} cm^{-2}) and the solvent (ξ_{H2O} = 9.42 × 10^{10} cm^{-2}), respectively. V_s and V_c are the volumes of the core block and the corona block, respectively. Given the mean number of repeat units in the core block and the corona block (100 and 113, respectively), and the mass densities of the PHPMA and PEG blocks (ρ_{PHPMA} = 1.21 g cm^{-3} and ρ_{PEG} = 1.23 g cm^{-3}, respectively, these solid-state values were measured at room

temperature, 21 °C, using a helium pycnometer) the volumes can be calculated from $V = \frac{M_w}{N_A \rho}$ as 29.7 nm^3 and 6.7 nm^3, respectively. The micelle aggregation number N_{agg} is given by the expression

$N_{agg} = (1 - x_{sol}) \frac{4\pi R_s^3}{3V_s}$, where x_{sol} is the concentration of water within the core. The amplitude of the core self-term is $A_s(q, R_s) = \Phi(qR_s) \exp\left(-\frac{q^2\Sigma^2}{2}\right)$, where $\Phi(qR_s) = \frac{3[\sin(qR_s) - qR_s \cos(qR_s)]}{(qR_s)^3}$ is the form factor amplitude of a sphere. The exponent term represents a sigmoidal interface between the blocks with a width Σ and a decaying scattering length density at the core surface. This parameter was fixed at 0.5 nm during data-fitting. The self-correlation term of the corona block is expressed via the Debye function $F_c(q, R_g) = \frac{2[\exp(-q^2 R_g^2) - 1 + q^2 R_g^2]}{q^4 R_g^4}$. Since the PEG corona contribution to the scattering signal is comparable to the scattering from the PHPMA core [$(\beta_c / \beta_s)^2 \approx 0.068$], the amplitude of the corona chain form factor was obtained from a normalized Fourier transform of the radial density distribution function of the PEG corona chains:

$$A_c(q) = \frac{\int_{R_s}^{R_s+2s} \mu_c(r) \frac{\sin(qr)}{qr} r^2 dr}{\int_{R_s}^{R_s+2s} \mu_c(r) r^2 dr} \exp\left(-\frac{q^2\Sigma^2}{2}\right) \qquad \text{(S2)}$$

The radial profile, $\mu_c(r)$, is expressed by a linear combination of two cubic B-splines with two fitting parameters *s* and *a* corresponding to the width of the profile and the weight coefficient, respectively. This information can be found elsewhere[4], as can the approximate integrated expression for Eq. (S2). A formalism used for the scattering intensity of interacting micelles:[3]

$$I = F_{mic}(q) + F_{mic}^{av}(q)[S(q) - 1] \qquad \text{(S3)}$$

was applied to derive form factors of both micelle dimers and micelle trimers. Thus the relative scattering intensity of a mixture of unimer micelles, dimer micelles and trimer micelles can be expressed as

$$I = F_{mic}(q)\sum_{n=1}^{3} k_n + F_{mic}^{av}(q)\sum_{n=2}^{3} nk_n[S_n(q)-1] \qquad \text{(S4)}$$

where n is the number of spheres forming unimers, dimers or trimers, and k_n is the volume fraction of each nano-object, $\sum_{n=1}^{3} k_n = 1$. The form factor for the average radial scattering length density distribution of spherical micelles indicated in both Eq. (S3) and Eq. (S4) is given by:

$$F_{mic}^{av}(q) = N_{agg}^2 \beta_s^2 A_s^2(q, R_s) + N_{agg}(N_{agg}-1)\beta_c^2 A_c^2(q) + 2N_{agg}^2 \beta_s \beta_c A_s A_c(q) \qquad \text{(S5)}$$

The form factor for both dimer micelles and trimer micelles [eq. (S4)] includes the Debye equation:[5]

$$S_n(q) = 1 + \frac{2}{n}\sum_{i=1}^{n-1}\sum_{j=i+1}^{n}\frac{\sin(qr_{ij})}{qr_{ij}} \qquad \text{(S6)}$$

where the inter-micelle separation distances are $r_{12} = r_{23} = 2(R_s + R_g)$ and $r_{13} = 4(R_s + R_g)$. Due to a possible partial interpenetration of the coronal chains on adjacent micelles, R_g (rather than $2R_g$) is used in the expressions for the inter-micelle separation distances. Size polydispersity of the micelles was determined assuming a normal distribution of the core radius (R_s).The spherical micelle model, Eq. (S4), produces a reasonably good fit to the SAXS data and mostly overlaps with the sphere model fitting (Figure S6). Programming tools for the Irena SAS Igor Pro macros were used for the model fitting, which yielded R_s = 12.2 nm, R_g = 1.8 nm, s = 3.3 nm and a = 3.1. It was also found that x_{sol} = 0.50, suggesting a relatively high degree of hydration for the plasticized PHPMA chains. However, this observation is consistent with our earlier ^{1}H NMR spectroscopy studies.[6] A similarly high value was also observed for Pluronic-type block copolymers.[4] It was also found that single spherical micelles dominate the PEG_{113}-$PHPMA_{100}$ aqueous dispersion (volume fraction ~ 0.9) with only a minor population of dimers and trimers (total volume fraction, $k_2 + k_3$ = 0.1). Fitting the SAXS pattern obtained after 1 second of X-ray exposure indicated that the proportion of dimers and trimers increased

significantly (k_2 + k_3 = 0.8). The core radius also slightly increased to 12.8 nm, presumably owing to thermal expansion and possible salvation.

If the micelle diameter is expressed as $2(R_s + R_g)$, the fitted sphere diameters (see Table 1) are close to the micelle diameters (27.4 nm vs. 28.0 nm and 28.8 nm vs. 29.2 nm). Some deviations are no doubt caused by the relative lack of definition of the interface between the corona block and the solvent compared to that used for the spherical micelle model. At it has already been mentioned, one reason for the success of the simplified sphere model is that the scattering length densities of the PEG and PHPMA blocks are similar, thus the micelles can be described as uniform spherical particles, rather than core-shell particles. This comparison justifies significant simplification of the SAXS analysis used in this work for the other self-assembled structures, since various details of the diblock copolymer morphologies can be neglected. Thus both worm-like micelles and vesicles formed by PEG-PHPMA diblocks in water can be represented as a homogeneous worm-like chain and a homogeneous membrane layer, respectively.

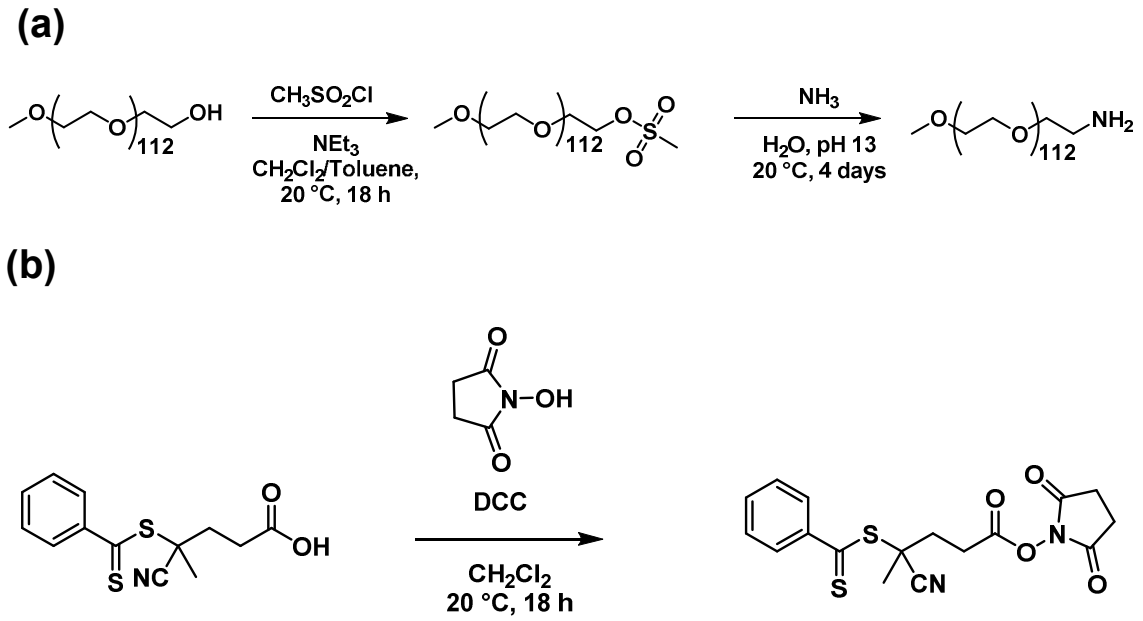

Scheme S1. (a) Conversion of monohydroxy-functionalized PEG starting material into the mono-aminated precursor via a mesylate intermediate. (b) Synthesis of 4-cyano-4-((thiobenzoyl)sulfanyl) pentanoic succinimide ester [SCPDB] via carbodiimide coupling of the commercially available cyanopentanoic acid dithiobenzoate with *N*-hydroxysuccinimide using dicyclohexyl carbodiimide (DCC) as the coupling agent.

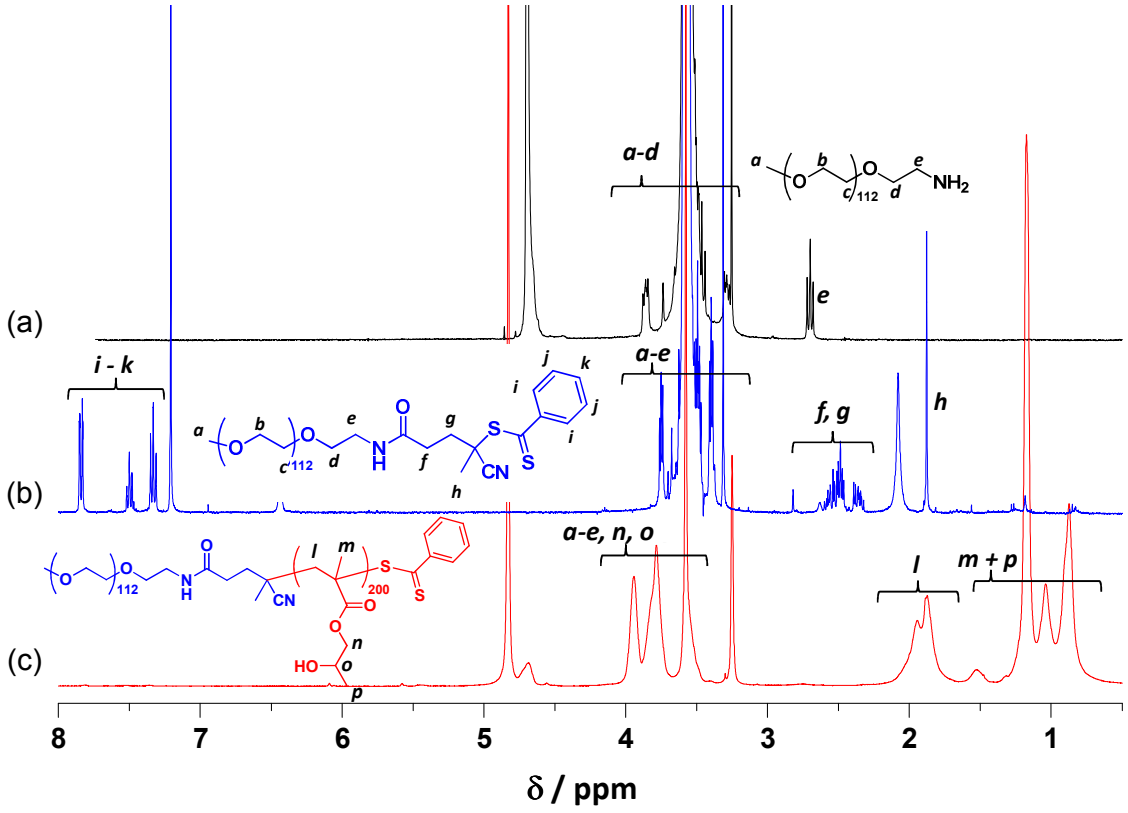

Figure S1. ^{1}H NMR spectra recorded for: (a) mono-aminated poly(ethylene glycol)$_{113}$ monomethyl ether; (b) PEG$_{113}$-DB macro-CTA synthesized by reacting SCPDB with mono-aminated poly(ethylene glycol)$_{113}$ monomethyl ether; (c) a PEG$_{113}$-PHPMA$_{200}$ diblock copolymer synthesized via RAFT aqueous dispersion polymerization.

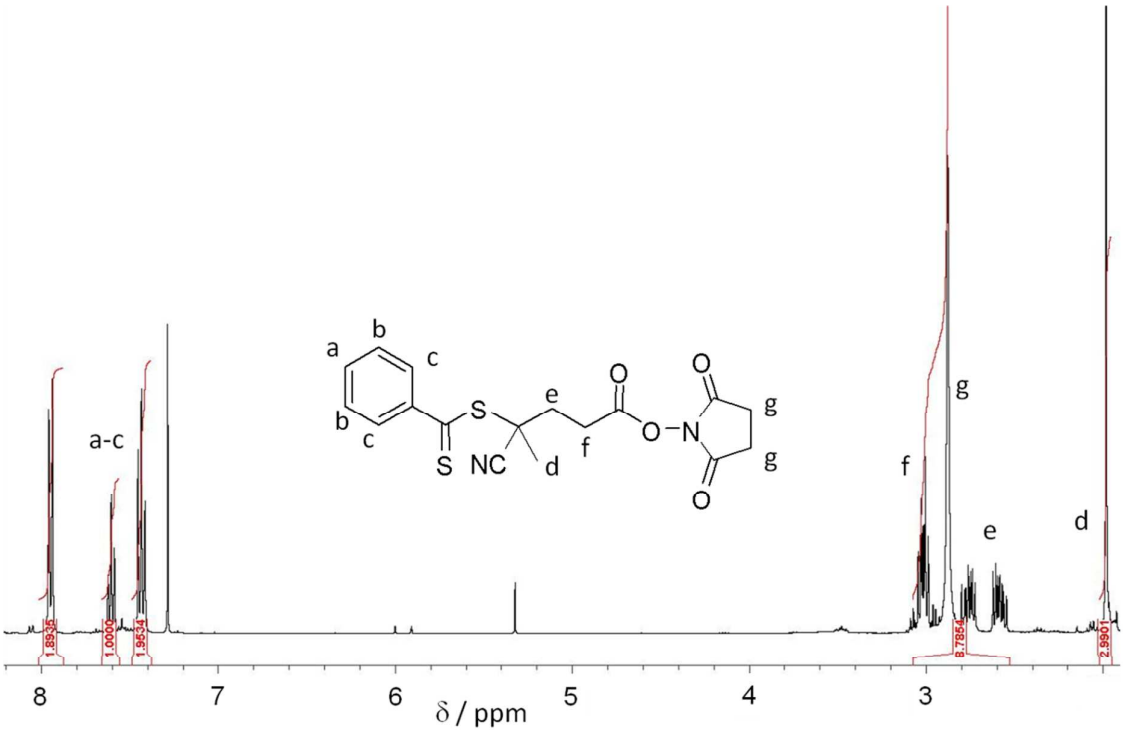

Figure S2. ^{1}H NMR spectrum ($CDCl_3$) recorded for SCPDB.

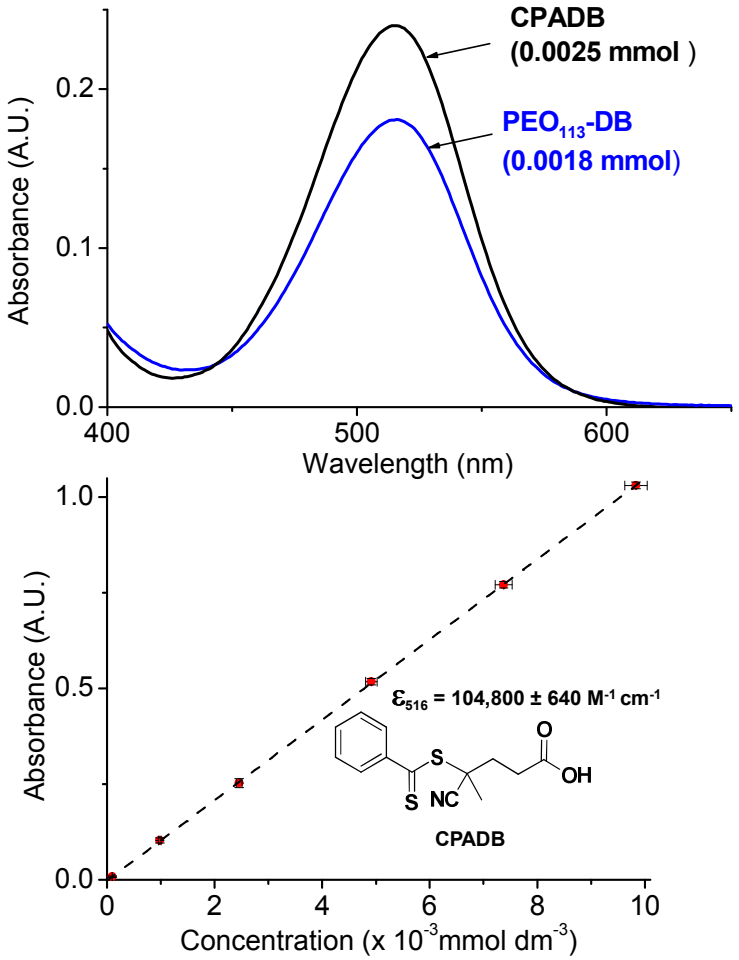

Figure S3. (a) Comparative visible absorption spectra recorded for the PEG_{113} macro-CTA and the CPADB CTA precursor. (b) Beer-Lambert linear calibration plot obtained for CPADB used to calculate the degree of functionalization of each PEG_{113} macro-CTA.

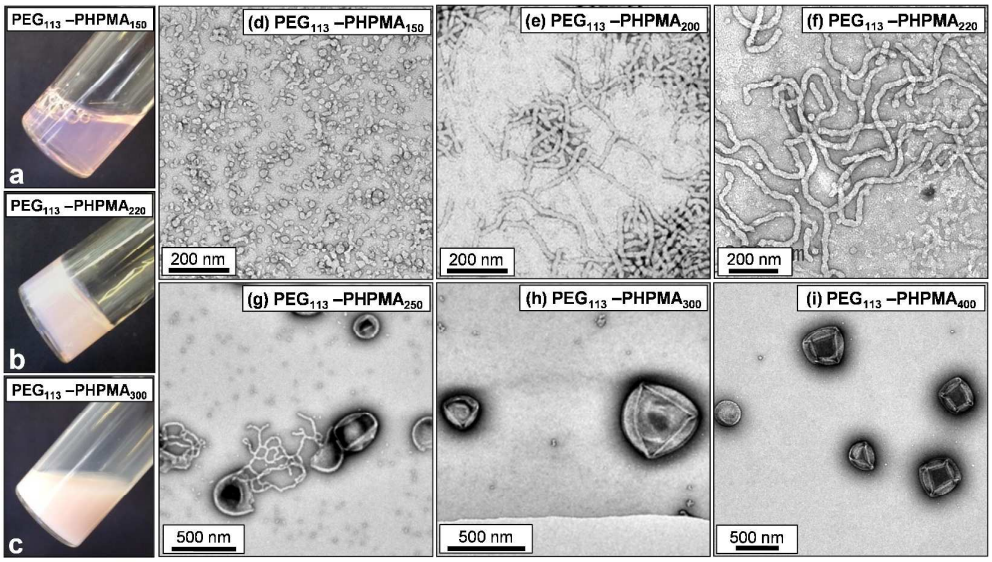

Figure S4. Digital images (a-c) and TEM images (d– i) obtained for selected PEG_{113}-$PHPMA_x$ dispersions synthesized at 10% w/w solids.

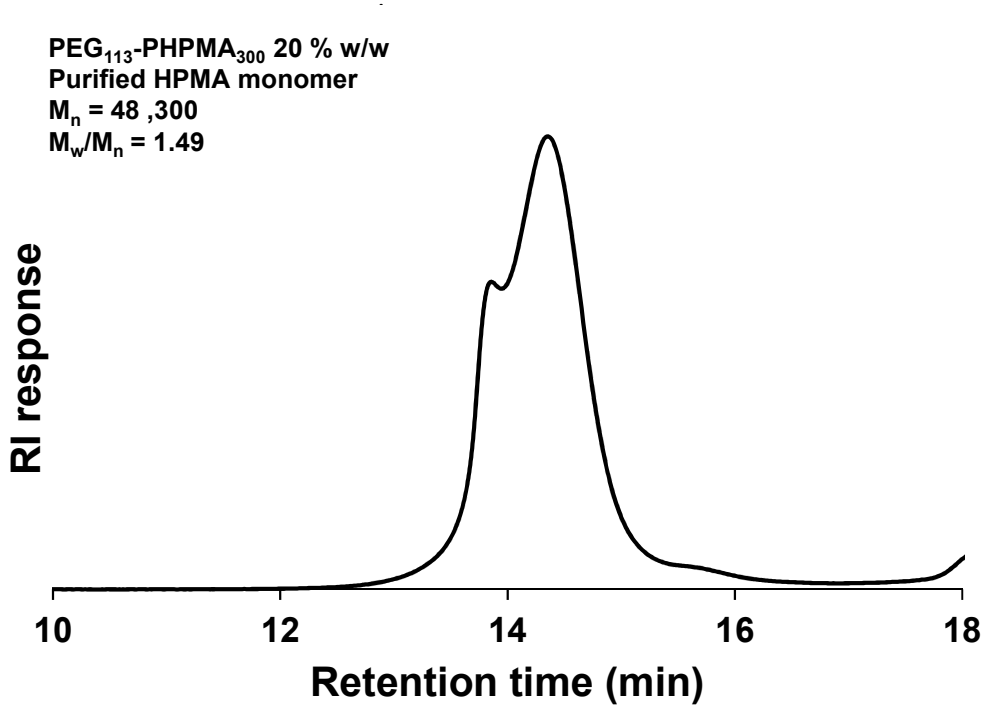

Figure S5. THF GPC chromatogram obtained for a PEG_{113}-$PHPMA_{300}$ diblock copolymer synthesized at 20% w/w solids.

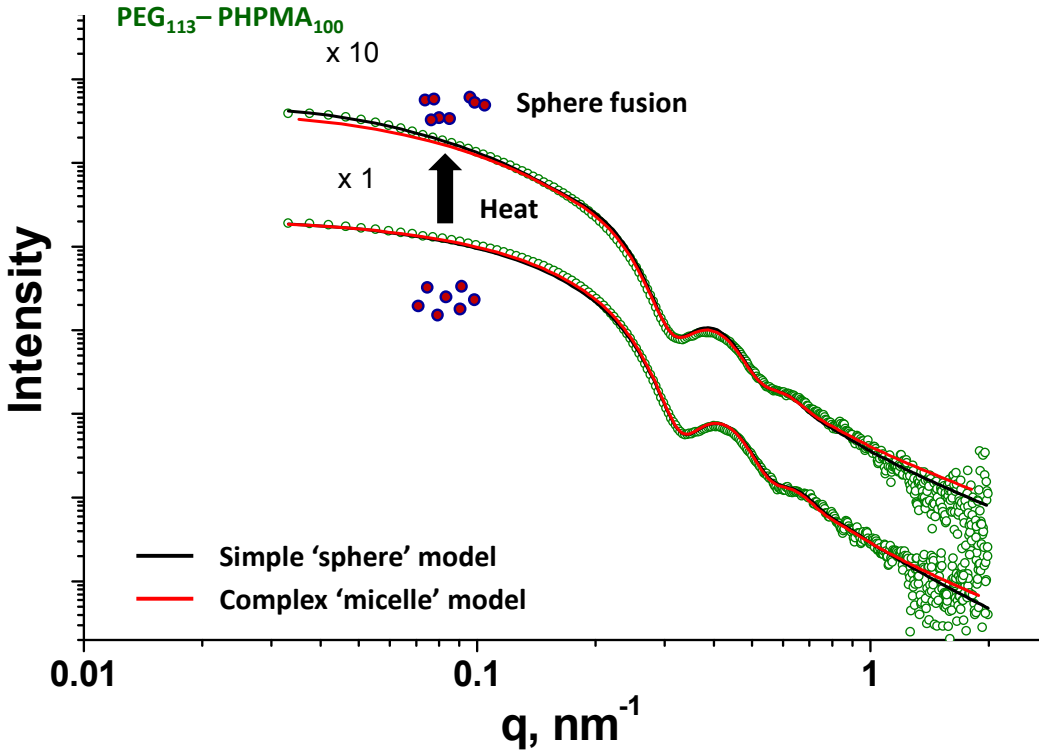

Figure S6. Fitting curves using two different models [sphere, Eq. (1), black line and sphere micelle, Eq. (S4), red line] are shown for PEG_{113}-$PHPMA_{100}$ data (green circles). The lower SAXS pattern represents the initial state of the sample (1st frame of the multi-frame acquisition). The upper SAXS pattern corresponds to a 1.0% w/w dispersion of PEG_{113}-$PHPMA_{100}$ exposed to the synchrotron x-ray beam continuously for 1 second (10th frame of the multi-frame acquisition).

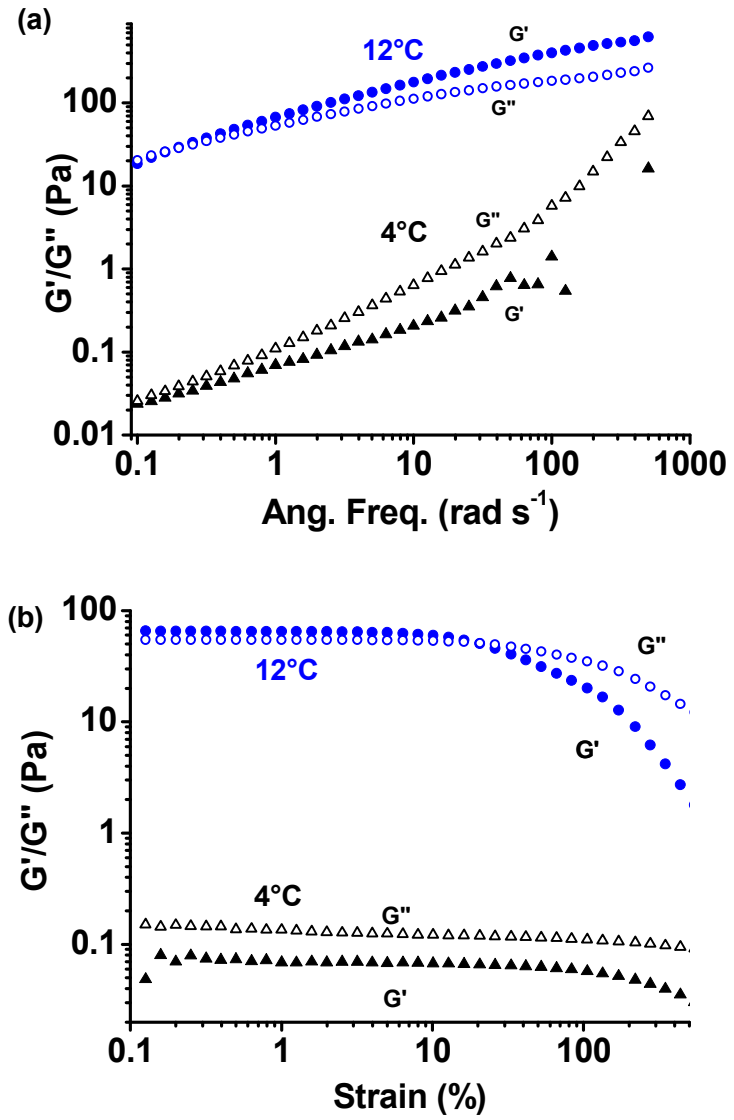

Figure S7. (a) Angular frequency dependence and (b) strain dependence on G' and G" for a PEG_{113}-$PHPMA_{220}$ dispersion at 12°C (worm gel) and 4°C (free-flowing liquid).

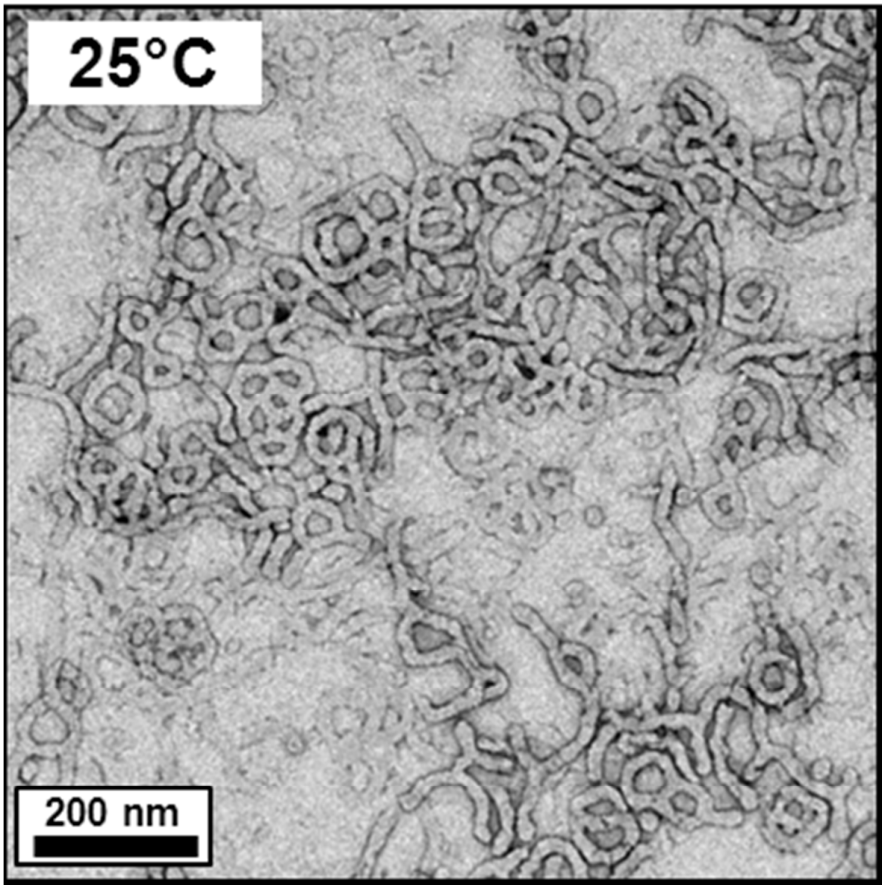

Figure S8. TEM image of a PEG_{113}-$PHPMA_{220}$ gel at 25°C after the reversilble temperature cycle.

PHPMA DP	Concentration % w/w	Conversion %	M_n g mol^{-1}	M_w/M_n	DLS diameter nm (PDI)	Morphology
PEG_{113} CTA	-	-	8,000	1.08	-	-
100	5	100	20,600	1.21	36 (0.19)	Spheres
200	5	100	29,900	1.23	130 (0.08)	Spheres, worms and vesicles
300	5	100	40,400	1.24	183 (0.10)	Spheres and vesicles
400	5	100	51,300	1.26	246 (0.12)	Spheres and vesicles
200	7.5	100	28,800	1.13	785 (0.26)	Worms
300	7.5	100	45,100	1.12	320 (0.08)	Vesicles
100	10	100	19,600	1.17	26 (0.06)	Spheres
150	10	100	25,000	1.19	36 (0.06)	Spheres
180	10	100	27,100	1.20	38 (0.29)	Spheres and worms
200	10	>99	29,100	1.19	747 (0.33)	Worms
220	10	>99	33,600	1.16	685 (0.30)	Worms
250	10	100	35,200	1.22	252 (0.27)	Worms and vesicles
300	10	>99	46,300	1.39	359 (0.05)	Vesicles
400	10	98	57,200	1.78	377 (0.07)	Vesicles
180	12.5	100	26,100	1.22	154 (0.21)	Spheres and Worms
200	12.5	100	30,100	1.23	750 (0.25)	Worms
100	15	100	19,600	1.17	31 (0.04)	Spheres
150	15	100	25,900	1.18	34 (0.04)	Spheres
180	15	100	27,000	1.20	95 (0.25)	Worms
200	15	100	31,500	1.19	447 (0.49)	Worms
220	15	>99	34,700	1.29	503 (0.14)	Worms and vesicles
250	15	>99	36,700	1.30	530 (0.25)	Worms and Vesicles
300	15	98	47,000	1.32	650 (0.16)	Vesicles
400	15	>99	66,500	1.86	2235 (0.53)	Vesicles
200	17.5	>99	30,100	1.21	752 (0.22)	Worms
220	17.5	>99	36,200	1.28	283 (0.12)	Worms and vesicles
300	17.5	>99	52,200	1.38	1030 (0.42)	Vesicles
100	20	>99	20,100	1.22	31 (0.04)	Spheres
150	20	>99	25,700	1.24	99 (0.22)	Spheres and Worms
180	20	>99	28,200	1.31	167 (0.29)	Worms
200	20	>99	33,100	1.33	578 (0.26)	Worms, vesicles and lamellar sheets
220	20	>99	34,500	1.38	3609 (0.50)	Giant vesicles
250	20	>99	38,400	1.84	1944 (0.45)	Giant vesicles and lamellar sheets
300	20	92	46,000	3.8	-	Giant vesicles and lamellar sheets
400	20	94	81,300	18.67	-	Precipitate

Table S1. Characterization data obtained for various PEG_{113}-$PHPMA_x$ diblock copolymer dispersions. These data were used to construct the detailed phase diagram shown in Figure 4 of the main text.

References

1. Ilavsky, J.; Jemian, P. R., Irena: tool suite for modeling and analysis of small-angle scattering. *Journal of Applied Crystallography* **2009**, 42, 347-353.
2. J. Kohlbrecher and I. Bressler, *SASfit*, https://kur.web.psi.ch/sans1/SANSSoft/sasfit.html (**2008**)
3. J. S. Pedersen, *J. Chem. Phys.*, **2001**, 114, 2839-2846.
4. J. S. Pedersen and M. C. Gerstenberg, *Colloids Surf., A*, **2003**, 213, 175-187.
5. L. A. Feigin and D. I. Svergun, *Structure Analysis by Small-Angle X-Ray and Neutron Scattering*, Plenum Press, New York, **1987**
6. A. Blanazs, R. Verber, O. O. Mykhaylyk, A. J. Ryan, J. Z. Heath, C. W. I. Douglas and S. P. Armes, *J. Am. Chem. Soc.*, **2012**, 134, 9741-9748.